JOURNAL OF PROTEOMICS 75 (2012) 2038–2052

Available online at www.sciencedirect.com

SciVerse ScienceDirect

www.elsevier.com/locate/jprot

# Quantitative proteomic analysis of okadaic acid treated mouse small intestines reveals differentially expressed proteins involved in diarrhetic shellfish poisoning

*Juan Wang, Yu-Yu Wang, Lin Lin, Yue Gao, Hua-Sheng Hong, Da-Zhi Wang**

*State Key Laboratory of Marine Environmental Science, Xiamen University, Xiamen 361005, China*
*College of the Environment and Ecology, Xiamen University, Xiamen 361005, China*

ARTICLE INFO

*Article history:*
Received 14 April 2011
Accepted 6 January 2012
Available online 16 January 2012

*Keywords:*
Okadaic acid
Diarrhetic shellfish poisoning
Protein phosphatase
Ultrastructure
Proteomics
Two-dimensional difference gel electrophoresis

ABSTRACT

Okadaic acid (OA) is a principal diarrhetic shellfish poisoning toxin produced by marine dinoflagellates. This study compared protein profiles of mice small intestines at four time points (0, 3, 6 and 24 h) after a single oral administration of 750 μg/kg OA, and identified the differentially expressed proteins using 2-D DIGE and MALDI-TOF-TOF mass spectrometry. The results showed that the toxin content of the intestines reached its peak 3 h after oral administration and then decreased rapidly. OA remarkably inhibited the intestinal PP activity but it recovered to the normal levels within 6 to 24 h. Electron microscope revealed the collapse of the villous architecture and the intestinal microvilli fell off at 3 h, but were repaired within 24 h. Notable damage to the intestinal ultrastructure was observed after oral administration. Comparison of the small intestine protein profiles at four time points revealed that 58 proteins were remarkably altered in abundance, and these proteins were involved in macromolecular metabolism, cytoskeleton reorganization, signal transduction, molecular chaperoning and oxidative stress, suggesting that OA toxicity in mouse intestines was complex and diverse, and that multiple proteins other than PP were involved in the diarrhetic process. Villin 1 and hnRNP F might be the key triggers inducing diarrhea in the mouse small intestines.



## 1. Introduction

Diarrhetic shellfish poisoning (DSP) is a gastrointestinal illness of worldwide distribution through the ingestion of filter feeding bivalves contaminated by the dinoflagellates *Dinophysis* spp. and *Prorocentrum* spp. [1], which can produce diarrhetic shellfish toxins, a type of lipophylic natural biotoxin [2]. Over the past few decades, the outbreak of DSP has increased significantly all over the world and has become of worldwide concern to public health and the shellfish industry [3].

Among the diarrhetic shellfish toxins, okadaic acid (OA) is the principal DSP toxin and presents a rapid-onset diarrheogenic intoxication. The gastrointestinal symptoms of DSP typically begin within half an hour to a few hours after consumption of OA-contaminated shellfish, and the recovery from intestinal injuries is completed within 3 days [4,5]. It has been demonstrated that OA acts as an inhibitor of serine/threonine protein phosphatases (PPs), which are responsible for the diarrheogenic effects observed in animals, including humans, after ingestion of OA contaminated bivalves, and which can be attributed to the accumulation of phosphorylated proteins which regulate metabolism, transport and secretion in the membrane [6–8]. OA has been recognized as a general tumor promoter in various murine organs, including the skin, glandular stomach and liver, and has been identified with many cell transformation tests *in vitro* [9–11]. In addition, OA belongs to the class of

* *Corresponding author at:* State Key Laboratory of Marine Environmental Science, Xiamen University, Xiamen 361005, China. Fax: +86 592 2186055.
E-mail address: dzwang@xmu.edu.cn (D.-Z. Wang).

1874-3919/$ – see front matter © 2012 Elsevier B.V. All rights reserved.
doi:10.1016/j.jprot.2012.01.010

non-TPA-type tumor promoters, which do not bind to the phorbol ester receptors in cell membranes or activate protein kinase C *in vitro*.

A number of studies have been devoted to the cytotoxicity and genotoxicity of OA using different *in vitro* cell lines. OA induces apoptosis of SCC-25 cells *via* stimulating the expression of the Fas receptor and Fas ligand [12]. Parameswaran et al. [13] report that OA induces significant apoptosis through increasing cytoplasmic nucleosome-associated DNA fragmentation and stimulating caspase activity in cultured rat mesangial cells at different time points. However, due to the different experimental designs, the molecular effects on cell proliferation, apoptosis, and cell cycle progression induced by OA are incompatible [14–16], although the multiple genes and signaling pathways involved in the process have been revealed [17].

So far, almost all the knowledge concerning the toxicological mechanisms of OA have been obtained from *in vitro* assays and, although the toxic effects of OA have been described *in vivo* based on traditional toxicological indices and morphological changes [18,19], the precise toxicological mechanism of OA resulting in diarrhea and its subsequent effects in mammals are not well established. On the other hand, taking account of the multiple genes and signaling pathways involved in the molecular mechanistic basis for the effects induced by OA, further study of the toxic mechanisms, particularly at the proteomic and genomic levels should be carried out in order to elucidate the precise toxicological mechanism of OA *in vivo*.

Global techniques such as proteomics provide effective strategies and tools for toxicological studies. In contrast to conventional biochemical approaches that address one or a few specific proteins at a time, proteomic techniques allow simultaneous isolation and identification of hundreds to thousands of proteins in one sample. Two-dimensional difference gel electrophoresis (2D-DIGE) technology is a newly developed 2-D gel-based approach that employs three fluorescent succinimidyl esters, termed CyDyes, to differentially label proteins prior to electrophoretic separation [20]. Because of the sensitivity and extended linear dynamic range of these dyes, this technique facilitates not only the quantification over a comparatively wide dynamic range with high accuracy, but also enables relative quantification with reference to an internal standard, thereby also facilitating the analysis of an adequate set of biological replicates in order to obtain the most significant data on protein regulation. This technique has recently been applied for identifying biomarkers, designing novel drug targets, and monitoring therapeutic processes [21].

In the present study, male ICR mice were acutely treated with 750 μg/kg OA using a single administration by gavage. The protein profiles of the small intestines at four time points (0, 3, 6, and 24 h after treatment) were analyzed using the 2D-DIGE approach, and the differentially expressed proteins were identified using MALDI-TOF-TOF mass spectrometry. The toxin content as well as the PP activity and any ultrastructural changes in small intestines was also investigated. Furthermore, western blot was carried out to validate the protein expression patterns of villin 1, heat shock protein 90 (HSP90), keratin 19 (KRT19), heterogeneous nuclear ribonucleoprotein F (HnRNP F) and 14-3-3 protein. The purpose of this study was to investigate the acute toxicity of OA in mice at the proteomic level and, together with the ultrastructural analysis, to provide a new insight into the molecular mechanism of OA resulting in diarrhea in mammals.

## 2. Materials and methods

### 2.1. *Mice exposure experiment*

Adult male ICR mice (18.0 ± 1.0 g body weight) were purchased from the Experimental Animal Centre of Xiamen University (Xiamen, China) and used for the experiments according to the guidelines of the Xiamen University Animal Welfare Committee. Mice were housed in plastic cages with air conditioning (20–23 °C) under a 12 h light–dark cycle with free access to food and water that were supplied daily. After 2 days acclimation, the mice were divided into four groups (six mice per group) according to their body weights.

The dose of OA was determined based on our preliminary experiment and previously published OA data [19,22]. OA was dissolved in saline solution (0.9% NaCl) containing 1.8% ethanol (v/v). All mice were exposed to OA *via* single oral administration at a dose of 750 μg/kg body weight/day using a dosing volume of 20 mL/kg of body weight and then one group of six mice were sacrificed at each time interval, that is 0, 3, 6, and 24 h after oral administration of OA. The small intestine was dissected and one part was immediately frozen in liquid nitrogen and stored at −80 °C for proteomic, PP activity and toxin content analysis as well as western blot analysis of selected proteins. The other part was fixed in 3.0% glutaraldehyde for cell ultrastructure analysis.

### 2.2. *Toxin content analysis*

The OA content of the intestinal tissue was analyzed according to the reported methods [23,24], but with minor modification. Briefly, 0.5 mL of 80% methanol (MeOH) was added to 100 mg of intestinal tissue, and homogenized with an ultrasonic disrupter (Model 450, Branson Ultrasonics, Danbury, CT, USA) in an ice-bath for 5 min and then centrifuged (16,000 *g*) at 4 °C for 10 min. The pellet was extracted again using the same procedure. The two supernatants were pooled together and washed once with the same volume of hexane. The hexane layer was discarded and the aqueous methanolic solution was extracted twice with equal volumes of chloroform. The combined chloroform solutions were dried with anhydrous sodium sulfate and centrifuged. The supernatant was evaporated using Speed Vac Concentrator (Thermo Scientific, MA). The residue was resuspended in 0.5 mL 80% MeOH prior to analysis. The analysis of OA in intestinal tissue was carried out using Agilent 6460 Triple Quad LC/MS System (Agilent Co, USA), equipped with an electrospray ionization interface (ESI). Separation was achieved on a Merck Lichospher-100 RP-18 (5 μm, 150 mm × 3 mm I.D). Column temperature was kept at 30 °C. The mobile phase consisted of acetonitrile–0.1% acetic acid (70:30, v/v) and the flow rate was set at 250 μL/min. The MS was operated in negative ion mode for the detection of OA with an ESI source set at 500 °C. The collision energy was set at −70 V for the precursor/product ion combinations *m/z* 803.6/255.0. The toxin content was quantified using an OA standard and expressed as ng cellular OA per gram tissue weight.

### 2.3. PP activity analysis

The analysis of PP activity was conducted according to previous studies [25,26], and 100 mg of intestinal tissue was sonicated in 1 mL T-PER reagent (Pierce Biotechnology Inc., Rockford, IL, USA) in an ice-bath. The supernatant was recovered by centrifugation (16,000 *g*) at 4 °C for 20 min. Then, 35 μL of the intestinal homogenate was mixed with 5 μL of $NiCl_2$ (40 mM), 5 μL of 5 mg/mL bovine serum albumin (BSA, Sigma, USA) and 35 μL of phosphatase assay buffer (50 mM Tris–HCl, 0.1 mM $CaCl_2$, pH 7.4) and incubated at 37 °C for 10 min. After that, 120 μL of 100 μM 6, 8-difluoro-4-methylumbelliferyl phosphate (DiFMUP, Sigma, USA) was added and incubated at 37 °C for another 30 min. PP activity was analyzed using a fluorescence microplate reader (RF-5301PC, Shimadzu, Japan) at 355 nm (excitation) and 460 nm (emission).

### 2.4. Ultrastructure analysis

The small intestine of the individually sacrificed mice was fixed in a solution of 3.0% glutaraldehyde in 0.1 M phosphate buffer (pH 7.4) for 4 h at 4 °C. The fixed intestines were washed three times using 0.1 M phosphate buffer (pH 7.4) at 20 min intervals with periodic agitation, and postfixed in 1% osmium tetroxide for 2 h at 4 °C, followed by a phosphate buffer wash three times at 20 min intervals. After dehydration in alcohol, the intestines were embedded in Epon-Araldite. Ultra-thin sections (50–80 nm) were moved onto titanium grids, stained with uranyl acetate and lead citrate and examined with a transmission electron microscope (TEM, JET 1200, JEOL Ltd, Japan).

### 2.5. Protein extraction

For 2D-DIGE and western blot analysis, the small intestinal tissues of two mice in each group were pooled together as one protein sample, so there were three protein samples for each group. Frozen intestinal samples were pulverized to a fine powder in liquid nitrogen and suspended in 10% w/v trichloroacetic acid (TCA)/acetone for 1 h at 4 °C. After centrifugation at 19,000 *g* for 30 min at 4 °C, the supernatant was removed and the pellet was suspended in 20% w/v TCA/acetone for 30 min at 4 °C. The pellet was recovered by centrifugation at 19,000 *g* for 30 min at 4 °C and washed twice with 80% acetone (v/v) and once with ice-cold acetone. Residual acetone was removed in a Speed Vac for about 5 min. The protein pellet was dissolved in 100 μL rehydration buffer containing 30 mM Tris, 7 M urea, 2 M thiourea, and 4% CHAPS (Bio-Rad, USA). Insoluble material was removed after centrifugation at 19,000 *g* for 20 min at 10 °C and the supernatants were collected for 2D-DIGE and western blot analysis. Protein concentration was determined using a 2-D Quant kit (GE Healthcare, USA) following the manufacturer's instructions.

### 2.6. CyDye labeling

Protein labeling was performed according to reported methods [27]. Each experiment contained four groups repeated in triplicate, generating 12 individual samples that were co-resolved across six DIGE gels all coordinated using the same pooled sample internal standard to reduce inter-gel variation. Experiments utilizing 24 cm pH 4–7 IEF gradients (Bio-Rad, USA) containing 150 μg of total protein were equally divided between any two samples and an aliquot of the internal standard as follows: proteins in each sample were fluorescently tagged with a set of matched fluorescent dyes according to the standard protocol (GE Healthcare, USA) for minimal labeling. To eliminate any dye-specific labeling artifacts, three samples of each group were labeled with Cy3 or with Cy5, respectively. The pooled sample internal standard was always Cy2-labeled (Table 1). In each case, 400 pmol of dye was used for 50 μg of protein. Briefly, labeling was performed for 30 min on ice in darkness and the reactions were quenched with the addition of 1 μL of 10 mM L-lysine (Sigma, USA) for 10 min on ice under the same conditions.

### 2.7. 2-D DIGE

The pair of Cy3- and Cy5-labeled samples was combined and mixed with a Cy2-labeled pooled standard. The mixtures containing 150 μg of protein were brought up to a final volume of 450 μL with 1× rehydration buffer, after which 0.5% IPG buffer 4-7(GE healthcare, USA) was added and they were mixed thoroughly. The labeled samples were then applied to the strips on an Ettan IPGphor III Isoelectric Focusing System (GE Healthcare, USA). Isoelectric focusing was conducted for a total of 60 kV-h using the following conditions: 40 V for 5 h, 100 V for 6 h, gradient to 500 V in 30 min, gradient to 1000 V in 30 min, gradient to 2000 V in 1 h, gradient to 10,000 V in 1 h, and finally 10,000 V for 6 h. At the end of focusing, the IPG strips were equilibrated with 10 mL equilibration buffer containing 50 mM Tris (pH 8.8), 6 M urea, 30% glycerol (w/v), 2% SDS (w/v), 1% DTT (w/v) and a trace amount of bromophenol blue. The strips were then equilibrated for 17 min in this solution but without DTT and with 2.5% iodoacetamide (Bio-Rad, USA). For the second-dimension electrophoresis, the equilibrated strips were transferred onto 12.75% SDS-polyacrylamide gels cast on low fluorescence glass plates using an Ettan-DALT six system (GE Healthcare, USA). Electrophoresis was carried out at 1 W/gel for 30 min followed by 20 W/gel until completion at 10 °C.

The differentially labeled co-resolved proteomic maps within each DIGE gel were imaged at 100-μm resolution separately using dye specific excitation and emission wavelengths and an Ettan DIGE Imager (GE Healthcare, USA). Cy2-, Cy3-, and Cy5-labeled images of each gel were acquired at excitation/emission values of 488/520, 523/580, and 633/670 nm, respectively. Gels were scanned directly on the low fluorescence glass plates, and 16-bit image file format images were exported for DIGE

**Table 1 – Schematic overview of the 2D-DIGE experimental conditions.**

| Gel | Cy2 | Cy3 | Cy5 |
|---|---|---|---|
| 1 | Internal standard | 0 h | 3 h |
| 2 | Internal standard | 6 h | 24 h |
| 3 | Internal standard | 24 h | 0 h |
| 4 | Internal standard | 3 h | 6 h |
| 5 | Internal standard | 0 h | 6 h |
| 6 | Internal standard | 24 h | 3 h |

data analysis. After imaging for CyDye, the gels were removed from the plates and subjected to silver staining.

### 2.8. DIGE image analysis

The DeCyder version 6.5 suite of software tools (GE Healthcare, USA) was used for DIGE analysis. The Differential In-gel Analysis (DIA) module was used for automatic spot detection and abundance measurements for each individual gel by comparing the normalized volume ratio of each protein spot from a Cy3- or Cy5-labeled sample on a given gel relative to the Cy2 signal from the pooled sample internal standard corresponding to the same spot feature. The DIA data sets from each individual gel were collectively analyzed using the biological variation analysis (BVA) module, which allows inter-gel matching and calculation of average abundance for each protein spot among the DIGE gels of this study. Statistical significance was assessed for each change in abundance using Student's *t*-test and analysis of variance (ANOVA) to compare the variation of expression within a group to the magnitude of change between groups. Based on a standardized average spot volume ratio, proteins whose abundance presented a relative change of 1.5 times or greater (either increase or decrease) among the four time points at 95% confidence level ($p<0.05$) were considered to be significant. Those protein spots with significant relative change across two or more time points were selected for further protein identification.

### 2.9. Silver staining

Sliver staining was performed following the method of Wang et al. [28]. Briefly, the gel was fixed for 2 h in a fixed solution containing 40% (v/v) ethanol and 10% (v/v) acetic acid and then transferred to a sensitizing solution containing 0.05% (w/v) sodium thiosulphate. The gel was washed by Milli-Q water three times for 5 min each time. Then the gel was stained in a 0.20% (w/v) silver nitrate solution with 0.015% (v/v) formaldehyde for 20 min and washed twice with Milli-Q water (15 s each time). The gel was developed with 2.5% (w/v) sodium carbonate containing 0.0074% (v/v) formaldehyde for 15 min, followed by the addition of 1.5% (w/v) ethylenediaminetetraacetic acid, disodium salt to stop the reaction. Finally, the gel was washed three times with Milli-Q water.

### 2.10. Protein identification

The differentially expressed protein spots were manually excised from silver stained DIGE gels and identified using MALDI-TOF-TOF MS as previously described [29]. Briefly, the spots were washed twice with 200 mM ammonium bicarbonate in 50% acetonitrile/water for 20 min at 30 °C, dehydrated with acetonitrile and then spun dried. In-gel trypsin digestion was carried out with 20 ng/μL trypsin (Roche, USA) in 25 mM ammonium bicarbonate overnight at 37 °C. After trypsin digestion, 1 μL of the peptide mixture was spotted on the target plate with 1 μL of 100 mM α-cyano-4-hydroxy-cinnamic acid in 50% acetonitrile and 0.1% trifluoroacetic acid and then dried. Finally, MALDI mass spectrometry was performed using an AB SCIEX 5800 MALDI TOF/TOF™ MS (Applied Biosystems, USA). MALDI-TOF MS and TOF-TOF tandem MS were performed and data were acquired in the positive MS reflector mode with a scan range from 850 to 4000 Da, and five monoisotopic precursors (S/N >50) were selected for MS/MS analysis. For interpretation of the mass spectra, a combination of peptide mass fingerprints and peptide fragmentation patterns were used for protein identification in an NCBI non-redundant database (selected for *Mus musculus*, 15,720 entries, updated on October 18, 2010) using the Mascot search engine (version 2.2, Matrix Science, London, UK). The raw MS and MS/MS spectra were processed using GPS Explorer software (Version 3.5, Applied Biosystems, USA) with the following criteria: minimum S/N: 10; peak density filter: 50 peaks per 200 Da; maximum number of peaks: 65; MS/MS peak filtering-mass range: 60–200 Da. Search parameters were set as follows: taxonomy: *M. musculus* (NCBInr); enzyme: trypsin; monoisotopic/average: monoisotopic; missed cleavage sites allowed: 1; fixed modification: carbamidomethyl; variable modifications: oxidation of methionine; fragment mass tolerance: 0.25 Da; peptide mass tolerance: 50 ppm; MS/MS ion tolerance: 0.1 Da. Results with C.I.% values greater than 95% were considered to be a positive identification. The identified proteins were then matched to specific processes or functions by searching Gene Ontology (GO) (www.geneontology.org).

### 2.11. Immunoblot analysis

To further validate the 2-D DIGE results, five proteins, villin 1, HSP90, KRT19, HnRNP F and 14-3-3 protein were selected for western blot analysis based on their higher fold difference on DIGE analysis and their potential roles in inducing the diarrhea. 30 μg protein for each protein sample was incubated in 95 °C for 5 min and separated on 12.0% SDS-polyacrylamide gels (Hoefer SE 600 Ruby, GE Healthcare, USA) using Laemmli buffer system. Proteins were transferred to polyvinylidene difluoride (PVDF) membrane (Millipore, Bedford, MA) using Trans-Blot SD Semi-Dry Transfer Cell (Bio-Rad, USA) at 200 mA for 3 h. Membranes were blocked with 5% non-fat dry milk for 2 h and then incubated with the primary antibodies for 2 h at room temperature as follows: anti-villin (1:1000 dilution; Abcam), anti-HSP90 (1:1000 dilution; Abcam), anti-KRT19 (1:1000 dilution; Abcam), anti-14-3-3 (1:1000 dilution, Santa Cruz), anti-HnRNP F (1:1000 dilution, Santa Cruz), and anti-GAPDH (1:1000 dilution, Santa Cruz). Following three washes in PBS containing 0.05% Tween 20 (PBST), the membranes were incubated with a secondary anti-rabbit or mouse IgG (1:5000; Jackson ImmunoResearch Laboratories, West Grove, PA) for 1 h at room temperature and then washed five times in PBST. Finally, the membranes were incubated with peroxidase-labeled streptavidin–biotin complex (Nichirei Bioscience Inc., Tokyo, Japan) for 10 min. The images of immunoblots were visualized using the Enhanced Chemiluminescent Substrate (Invitrogen) and the intensity of the bands was determined by densitometric analysis. The target protein signals were normalized to the GAPDH signal and analyzed semiquantitatively using Quantity One system.

### 2.12. Statistical tests

All measurements were replicated at least three times and all values were expressed as mean values±standard deviation. For the analysis of protein expression in 2-D DIGE, the significant difference between four groups was analyzed as described

above. For PP activity, OA content and western blot analysis, the raw data were analyzed using SPSS for Windows 13.0 Software (SPSS, Inc) and determined with a one-way ANOVA analysis followed by the Bonferroni multiple range test and Student's t-test to evaluate whether the means were significantly different among the groups. Significant differences were indicated when the probability was less than 0.05 ($p<0.05$).

## 3. Results

### 3.1. Symptoms and lethality

Two hours after a single oral administration of an OA dose of 750 μg/kg, the mice were motionless, and they presented diarrhea and reduction of food consumption 3 h after oral administration. Body weight loss was observed 24 h after oral administration, but no mouse died during the 24 h experimental period. Necroscopic analysis of OA-treated mice showed that both the small and large intestines were hyperemic and contained a pale fluid 3 h, 6 h and 24 h after oral administration.

### 3.2. Toxin content and PP activity in mouse intestines

The toxin contents in the mice intestinal tissues at the four time points are shown in Fig. 1. No OA was detected in the intestinal tissues immediately after oral administration. However, the toxin content reached its peak 3 h after oral administration (up to 798.05 ng/g intestinal tissue) and then it decreased rapidly and reached a low level at 24 h, indicating that OA was rapidly eliminated from the mice.

Variations of PP activity in the mice intestinal tissues at the four time points are shown in Fig. 2. The intestinal PP activity decreased significantly 3 h and 6 h after oral administration ($p<0.05$), and then recovered to the normal level by the end of the experiment (24 h).

### 3.3. Ultrastructural analysis

Variations in the intestinal microvilli and cellular ultrastructure of OA-treated mice were analyzed at the four time points. Electron microscopy revealed tightly packed, slender, and uniform-shaped microvilli on the surface of the intestinal epithelial cell at 0 h, but the microvilli were damaged markedly at 3 h and many microvilli were sloughed off (Fig. 3A). With increased time, the microvilli were repaired gradually and presented no significant difference from that at 0 h. For the cellular ultrastructure (Fig. 3B), dilation of the rough endoplasmic reticulum (rER) in the intestinal cells was observed 3 h after oral administration, while swelling, ridge disappearance and destroyed structure of the mitochondria were observed 6 h after oral administration. These ultrastructural changes were still observed even at the end of the experiment.

### 3.4. 2-D DIGE analysis of differential protein expression

Protein profiles of mice intestinal tissues at the different time points were analyzed using 2-D DIGE, and representative 2-D DIGE images of the different time point samples (0 h vs 3 h; 6 h vs 24 h) are shown in Fig. 4A. Based on the DIA module analysis, 2034±209, 2175±197, 2081±186 and 2111±224 protein spots were detected in the intestinal cells at 0, 3, 6, and 24 h, respectively. Among them, a total of 58 exhibited statistically significant alterations ($p<0.05$, ANOVA, $n=3$) and the variations in abundance were more than 1.5 fold. For the altered spots, 40 were detected localized in the 3 h vs 0 h gel (12 up-regulated proteins and 28 down-regulated proteins), and 38 were detected localized in the 6 h vs 0 h gel (3 up-regulated proteins and 35 down-regulated proteins). In addition, 34 of the 58 spots which showed alterations in protein abundance were detected localized in the 24 h vs 0 h gel (2 up-regulated protein and 32 down-regulated proteins) (Fig. 4B).

### 3.5. Protein identification and variation at different time points

All the protein spots showing alterations were submitted for identification using MALDI-TOF-TOF analysis and then searched in the NCBI mice database. The information concerning differentially expressed proteins of mice intestinal tissues is shown in Fig. 4B. Details of NCBI ID number, theoretical pI value, theoretical molecular weight, protein score, protein score C.I. %, as well

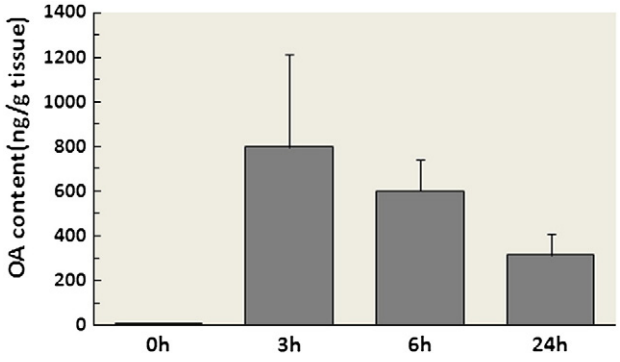


**Fig. 1 – OA content in the intestinal tissues of ICR mice at 0 h, 3 h, 6 h and 24 h after a single oral administration of OA (750 μg/kg body weight). Values are given as mean values ± SD ($n=6$).**

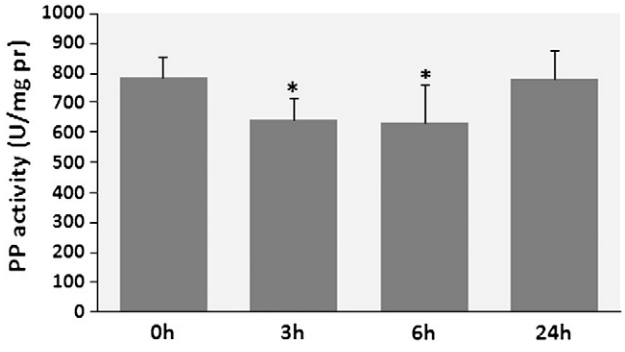


**Fig. 2 – PP activity in the intestinal tissues of ICR mice at 0 h, 3 h, 6 h and 24 h after a single oral administration of OA (750 μg/kg body weight). Values are given as mean values ± SD ($n=6$). $^{*}p<0.05$.**

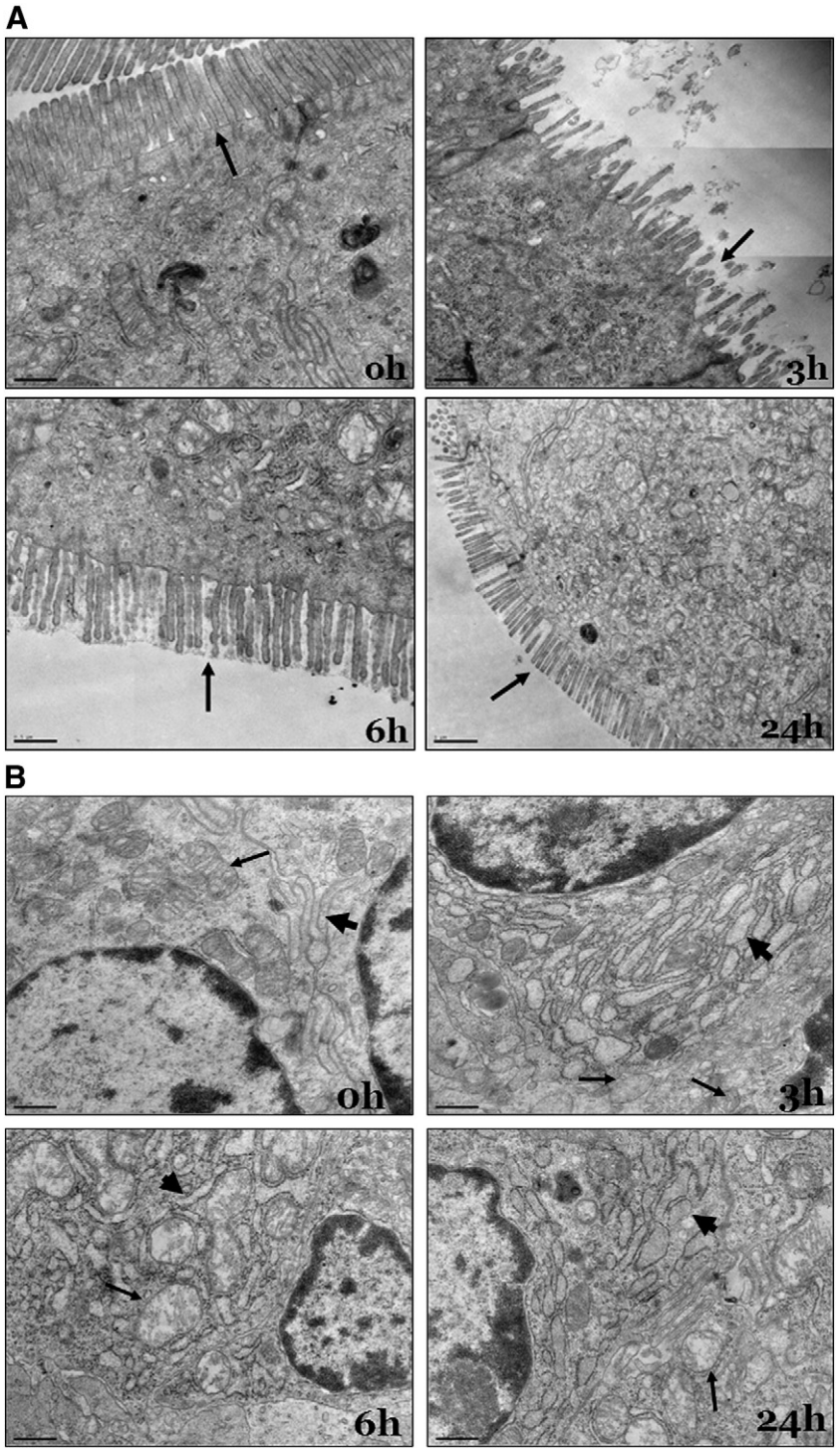


**Fig. 3 – Transmission electron micrographs of intestinal cells of ICR mice at 0 h, 3 h, 6 h and 24 h after a single oral administration of OA (750 μg/kg body weight). A: Microvilli (black arrow indicated); B: Mitochondria (black arrow indicated) and endoplasmic reticulum (black triangle indicated).**

as average relative change at each time point, for all identified proteins are listed in Table 2.

Based on GO classification, the 58 proteins were assigned into five functional groups, *i.e.* macromolecular metabolism (lipid, amino acid and sugar metabolism), molecular cytoskeleton reorganization, molecular chaperones, signal transduction, and oxidative stress (Fig. 5). Overall, the majority was seriously down-regulated after a single oral administration of OA. The 18 protein spots (31%) involved in macromolecular metabolism were altered in abundance: two digestive enzymes, chymotrypsin B1 precursor (spots 6 and 48) and trypsin 4 (spot 20) were down-regulated markedly during the whole experimental period. Fatty acid binding protein (spot 36) and retinol binding proteins (spots 37 and 38) decreased significantly in abundance at 3 h

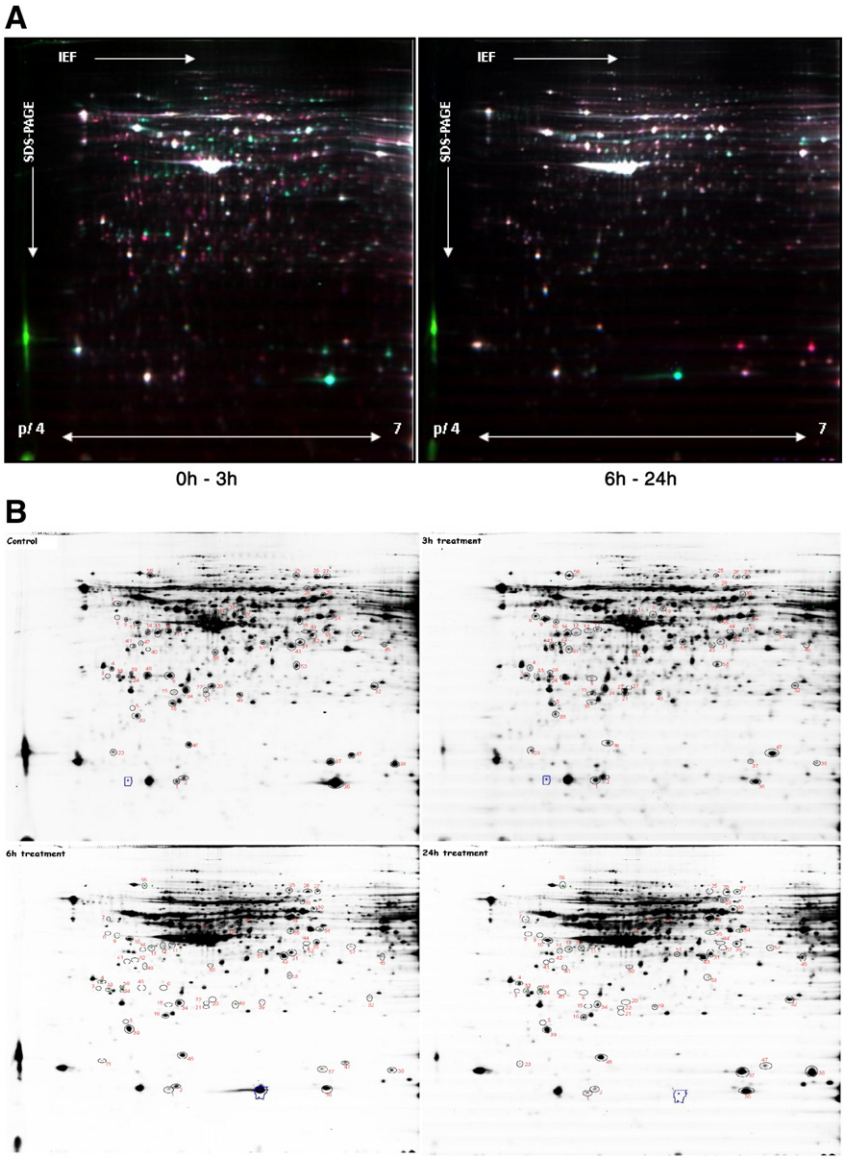


**Fig. 4 – 2-D DIGE analysis of intestinal cells at 0 h, 3 h, 6 h and 24 h after a single oral administration of OA (750 μg/kg body weight). A: Representative 2-D DIGE image for protein expression maps using a 12.75% homogeneous SDS-PAGE gel with the pH range from 4 to 7. B: Differentially expressed protein spots determined by DeCyder software. The molecular weights (MW) and p*I* scales are indicated. Each gel is representative of three independent replicates.**

and 6 h, but they recovered to the normal levels 24 h after oral administration. Four proteins, including phosphoglucomutase 1 (spot 28), fructose-1,6-bisphophatse (spot 31 and 51), and NADH dehydrogenase, flavoprotein 2 (spot 49), involved in glycometabolism were suppressed in protein expression 6 h and/or 24 h after oral administration, whereas six proteins, aminoacylase 1 (spot 35), spermidine synthase (spot 50), purine nucleoside phosphorylase (spot 53), adenosine kinase (spot 54), ornithine aminotransferase (spot 55), arginase type II(spot 57) related to amino acid metabolism were almost down-regulated during the whole experimental period. Eight protein spots believed to be molecular chaperones were changed in protein expression at 3 h and/or 6 h, including heat shock protein 90, t-complex protein and protein disulfide-isomerase A6. Seven oxidative stress protein spots, including galactose binding lectin, peroxiredoxin 2 (PRX2) and Cu/Zn superoxide dismutase (Cu/Zn SOD), were down-regulated by OA. Eleven cytoskeleton reorganization proteins, such as keratins (Keratin 7, 8 and 19), villin 1, myosin and actin were affected by OA; among them, EndoA' cytokeratin and villin 1 (spot 26 and 27) were down-regulated significantly during the whole experimental period. Three major groups of signal transduction proteins, 14-3-3 protein isoforms (epsilon, gamma and beta), eukaryotic translation initiation factors (eIFs) and heterogeneous nuclear ribonucleoprotein F (hnRNP F) were identified. Among them, four eIFs, eIF6 (spot 3), eIF4A1 (spot 18), eIF5A (spot 46) and eIF2 (spot 52) altered in abundance over time. eIF4A1 and eIF5A were down-regulated at 3 h, while eIF6 and eIF2 were down-regulated 6 h after OA treatment. Three 14-3-3 proteins (spots 4, 58 and 59) were down-regulated during the whole experimental period. However, hnRNP F (spots 21 and 22) was only induced 3 h after oral administration but it was not detected at other time points.

### 3.6. *Western blot analysis on villin 1, HSP90, KRT19, HnRNP F and 14-3-3 protein*

Western blot analysis was then conducted to validate the differentially expressed proteins villin 1, HSP90, KRT19, HnRNP F and 14-3-3 protein identified by 2-D DIGE. Results shown in Fig. 6 that indicated the changes in protein levels from the result of western blot were generally consistent with the variations from 2-D DIGE analysis. For example, the expression of villin 1 was down-regulated with the treatment of OA compared with the protein level of 0 h sample, while the changes in protein level of HSP90, KRT19 and HnRNP F were up-regulated at 3 h after OA treatment ($p<0.05$). The expression levels of 14-3-3 protein at four time points showed no significant change ($p>0.05$) compared to 2-D DIGE result.

## 4. Discussion

A number of studies demonstrate that the small intestine is the target organ of OA in mammals [30,31], and OA is detected in mouse small intestines 5 min after oral administration, and swollen intestinal villi and erosion are observed within 1 h. Other studies also report that OA causes edema in the upper part of the small intestine within 1 h, and results in hypersecretion and erosion, but that recovery from this damage occurs within 48 h. The present study confirmed the above findings: OA destroyed the intestinal microvilli to a remarkable extent and the microvilli became disorganized 3 h after oral administration. However, the damaged microvilli recovered gradually within 24 h (Fig. 3A). OA also resulted in the dilation of the rER in the intestinal cells as well as swelling, ridge disappearance and damaged mitochondrial structure. These results suggested that OA destroyed the microvilli structure and function, and subsequently the cellular ultrastructure of the small intestines, which resulted in their dysfunction.

The serine/threonine PPs are a group of enzymes that perform dephosphorylation of numerous proteins which regulate many essential metabolic processes in eukaryotic cells. The inhibition of serine/threonine PPs leads to the collapse of regulatory mechanisms and results in cell death [32]. OA can inhibit PP activity, which results in the accumulation of phosphorylated proteins and subsequently diarrhea in animals including humans. In the present study, intestinal PP activity declined significantly 3 h and 6 h after oral administration of OA, but it recovered to the normal level after 24 h. Our results suggested that the inhibition of PP by OA might be one trigger resulting in the diarrhea, but this adverse effect was short and PP activity recovered rapidly from OA toxicity.

The present study revealed that the 18 protein spots involved in various types of macromolecular metabolism (i.e. lipid, amino acid and sugar) were significantly down- or up-regulated at different time points after oral administration of OA. Among these proteins, fatty acid-binding protein (I-FABP, spot 36), an important cytosolic protein in small intestine epithelial cells, was down-regulated at 3 h in protein level. I-FABP participates in the uptake, intracellular metabolism and/or transport of long chain fatty acids [33]. Studies also show that OA can significantly disrupt the secretory processing of apolipoprotein B by increasing cellular protein phosphorylation in Caco-2 cells [34]. The down-regulation of I-FABP in our study suggested that OA might have interrupted the lipid metabolism and fatty acid transport of the intestine. Retinol-binding protein (RBP) is the sole specific transport protein for retinol (vitamin A) in circulation, and its single known function is to deliver retinol to the tissues [35]. Vitamin A performs a key role in maintaining the structural integrity of epithelial cells, and deficiencies of vitamin A could interrupt the biosynthesis of glycoprotein in mucosal cells, and then affect the physiological functioning of the mucosa. In our study, RBP2 (spots 37 and 38) was also down-regulated significantly at 3 h and 6 h, suggesting that OA destroyed the structural integrity of intestinal epithelial cells through inhibiting the transport of vitamin A. Moreover, the aldehyde dehydrogenase 1 family member L1 (spot 25), an enzyme involved in catalyzing the conversion of retinal to retinoic acid, was also down-regulated during the whole experiment, and retinol and retinoic acid could decrease squamous epithelization by regulating gene expression. Apart from these proteins, chymotrypsin B1 precursor (spot 6 and 48) and trypsin 4 (spot 20), two important proteolytic enzymes involved in the digestive systems of mammals, were noticeably down-regulated during the whole experimental period. Hence, we speculated that OA might destroy the absorptive functions of the intestinal epithelium through impairing the structure of intestinal cells and inhibiting the activities of digestive enzymes, and so result in diarrhea.

The presence of OA affected glycometabolism of the mouse small intestines in that four proteins involved in glycometabolism were altered in protein abundance during the experimental period. NADH dehydrogenase flavoprotein 2 (NDUFV2, spot 49) was down-regulated dramatically 6 h after oral administration, while phosphoglucomutase 1 (PGM1, spot 28) was significantly up-regulated at 3 h and down-regulated at 6 h and 24 h. NDUFV2 is the core subunit of the mitochondrial membrane respiratory chain, the NADH-ubiquinone oxidoreductase complex (complex I), that is believed to catalyze the transfer of electrons from NADH to ubiquinone. A previous study shows that the decrease of NDUFV2 can directly impair electron transport in the mitochondrial inner membrane, and then increase ROS and induce apoptosis [36]. PGM1 is an important regulatory enzyme in cellular glucose utilization and energy homeostasis, which catalyzes the interconversion of mannose-6-phosphate and mannose-1-phosphate in the early stage of the biosynthesis of lipid-linked oligosaccharides. The deficiency of PGM is responsible for a disorder called congenital disease of glycosylation 1a [37]. Our ultrastructure results also indicated the impairment of mitochondria 6 h after OA treatment. These results suggested that OA might induce the disorder of energy metabolism in mitochondria coupled with the apoptosis of intestinal cells.

In this study, six proteins associated with amino acid metabolism were down-regulated 6 h and 24 h after oral administration. Among these proteins, ornithine aminotransferase is a mitochondrial matrix enzyme that catalyzes a reversible reaction involving the interconversion of ornithine and glutamate semi-aldehyde, and is therefore involved in the metabolism of arginine and glutamine which play a major role in N homeostasis [38]. Ornithine is involved in the urea cycle, which processes the excess nitrogen generated when protein is broken down by the body. In addition to its role in the

**Table 2 – Differentially expressed proteins of intestinal cells at various time points after OA treatment.**

| Spot ID [a] | NCBI [b] | Protein name | Theoretical pI | Theoretical MW | No. of matched peptides | Sequence coverage (%) | Protein score | Protein score C.I.% | 3 h vs 0 h | | 6 h vs 0 h | | 24 h vs 0 h | |
|---|---|---|---|---|---|---|---|---|---|---|---|---|---|---|
| | | | | | | | | | Av. ratio [c] | *p* value | Av. ratio [c] | *p* value | Av. ratio [c] | *p* value |
| *Macromolecular metabolism* | | | | | | | | | | | | | | |
| 6 | 255522937 | Chymotrypsin B1 precursor | 4.91 | 28,431.0 | 10 | 54 | 499 | 100 | −7.34 | 0.006 | −7.58 | 0.004 | −6.01 | 0.005 |
| 20 | 6755893 | Trypsin 4 | 5.48 | 26,941.2 | 8 | 43 | 321 | 100 | −7.37 | 0.003 | −5.13 | 0.005 | −4.14 | 0.007 |
| 25 | 27532959 | Aldehyde dehydrogenase 1 family, member L1 | 5.64 | 99,501.9 | 35 | 52 | 1250 | 100 | −2.30 | 0.021 | −2.20 | 0.026 | −9.15 | 0.004 |
| 28 | 21410124 | Phosphoglucomutase1, isoform CRA_b | 5.78 | 69,072.4 | 19 | 35 | 444 | 100 | +3.15 | 0.017 | −1.80 | 0.054 | −4.78 | 0.006 |
| 31 | 122937183 | Fructose-1,6-bisphosphatse 2 | 5.90 | 37,209.0 | 14 | 35 | 416 | 100 | −3.12 | 0.007 | −1.02 | 0.926 | +1.17 | 0.480 |
| 35 | 148689188 | Aminoacylase 1 | 5.84 | 42,354.2 | 23 | 65 | 1210 | 100 | −3.98 | 0.004 | −1.29 | 0.461 | −1.98 | 0.038 |
| 36 | 6679737 | Fatty acid binding protein 2, intestinal | 6.62 | 15,116.7 | 7 | 46 | 336 | 100 | −2.87 | 0.005 | −2.77 | 0.006 | +1.19 | 0.010 |
| 37 | 255759938 | Retinol-binding protein 2 | 6.14 | 15,770.8 | 9 | 59 | 133 | 100 | −5.27 | 0.003 | −11.22 | 0.003 | +1.70 | 0.070 |
| 38 | 255759938 | Retinol-binding protein 2 | 6.14 | 15,770.8 | 6 | 44 | 125 | 100 | −5.25 | 0.003 | −5.19 | 0.005 | +1.81 | 0.053 |
| 45 | 188036180 | Chain A, crystal structure of 5-aminolevulinic acid dehydratase | 6.32 | 36,472.5 | 13 | 30 | 246 | 100 | −1.72 | 0.057 | −1.57 | 0.103 | +2.57 | 0.017 |
| 48 | 255522937 | Chymotrypsin B1 precursor | 4.91 | 28,431.0 | 9 | 59 | 902 | 100 | +1.12 | 0.599 | −6.41 | 0.004 | −7.45 | 0.002 |
| 49 | 12850902 | NADH dehydrogenase [ubiquinone] flavoprotein 2, mitochondrial precursor | 7.00 | 27,610.0 | 9 | 52 | 477 | 100 | −1.12 | 0.885 | −5.13 | 0.005 | −3.62 | 0.008 |
| 50 | 6678131 | Spermidine synthase | 5.31 | 34,543.0 | 11 | 43 | 513 | 100 | −1.47 | 0.171 | +1.88 | 0.046 | −4.44 | 0.006 |
| 51 | 122937183 | Fructose-1,6-bisphosphatase 2 | 5.90 | 37,209.0 | 15 | 44 | 402 | 100 | +1.78 | 0.148 | −2.41 | 0.020 | −1.36 | 0.183 |
| 53 | 7305395 | Purine nucleside phosphorylase | 5.78 | 32,527.0 | 18 | 58 | 1120 | 100 | −1.29 | 0.168 | −6.04 | 0.005 | −1.73 | 0.004 |
| 54 | 148669527 | Adenosine kinase, isoform CRA_a | 6.11 | 39,129.0 | 16 | 42 | 566 | 100 | +1.07 | 0.270 | −5.21 | 0.005 | −5.20 | 0.005 |
| 55 | 8393866 | Ornithine aminotransferase, mitochondrial precursor | 6.19 | 48,723.1 | 15 | 37 | 783 | 100 | +1.66 | 0.082 | −12.12 | 0.003 | −11.49 | 0.002 |
| 57 | 19484063 | Arginase type II | 6.20 | 39,195.2 | 13 | 50 | 716 | 100 | +1.10 | 0.784 | −3.04 | 0.012 | −2.18 | 0.027 |
| *Molecular chaperones* | | | | | | | | | | | | | | |
| 8 | 118142832 | HSP90 aa1 protein | 5.05 | 66,080.5 | 17 | 36 | 281 | 100 | +3.06 | 0.004 | −1.90 | 0.045 | −1.26 | 0.327 |
| 9 | 40556608 | Heat shock protein, HSP90 beta | 4.97 | 83,752.1 | 24 | 27 | 588 | 100 | +6.98 | 0.004 | −1.85 | 0.049 | −1.18 | 0.460 |
| 15 | 40556608 | Heat shock protein, HSP90-beta | 4.97 | 83,572.1 | 13 | 20 | 259 | 100 | +1.63 | 0.008 | −1.11 | 0.646 | −3.45 | 0.003 |
| 17 | 51455 | Heat shock protein 65 | 5.91 | 61,074.4 | 13 | 31 | 199 | 100 | −2.59 | 0.007 | +1.16 | 0.504 | +1.20 | 0.432 |
| 30 | 148670089 | t-complex protein, isoform CRA_b | 6.02 | 55,880.3 | 21 | 34 | 704 | 100 | −2.92 | 0.008 | −2.65 | 0.016 | +1.97 | 0.366 |
| 41 | 62510933 | Protein disulfide-isomerase A6 | 5.00 | 48,469.4 | 5 | 14 | 306 | 100 | +1.96 | 0.007 | −1.87 | 0.047 | −3.19 | 0.011 |
| 42 | 62510933 | Protein disulfide-isomerase A6 | 5.00 | 48,469.4 | 12 | 30 | 459 | 100 | +2.34 | 0.006 | −1.27 | 0.311 | −1.88 | 0.046 |
| 56 | 14714615 | Heat shock protein 90, beta | 4.74 | 92,717.4 | 38 | 52 | 1420 | 100 | −1.37 | 0.175 | −8.59 | 0.004 | −4.54 | 0.006 |

| | | | | | | | | | | | | | | |
|---|---|---|---|---|---|---|---|---|---|---|---|---|---|---|
| *Cytoskeleton* | | | | | | | | | | | | | | |
| 5 | 148672102 | Keratin 7 | 5.01 | 32,603.4 | 6 | 15 | 114 | 100 | +4.89 | 0.003 | −1.50 | 0.124 | −1.28 | 0.299 |
| 11 | 76779293 | Keratin 8 | 5.70 | 54,513.5 | 27 | 55 | 481 | 100 | −1.69 | 0.006 | −2.79 | 0.014 | −2.68 | 0.015 |
| 12 | 309215 | EndoA' cytokeratin, putative | 5.42 | 53,209.7 | 9 | 20 | 90 | 99.984 | −7.02 | 0.004 | −7.70 | 0.003 | −8.18 | 0.004 |
| 13 | 6680606 | Keratin 19 | 5.28 | 44,514.7 | 28 | 69 | 636 | 100 | −2.95 | 0.008 | −2.46 | 0.003 | −4.81 | 0.006 |
| 14 | 6680606 | Ketatin 19 | 5.28 | 44,514.7 | 20 | 51 | 425 | 100 | +1.78 | 0.056 | −4.57 | 0.003 | −5.77 | 0.005 |
| 26 | 190684696 | Villin-1 | 5.72 | 93,229.8 | 36 | 41 | 777 | 100 | −3.37 | 0.006 | −2.75 | 0.014 | −2.91 | 0.013 |
| 27 | 148667910 | Villin-1 | 5.77 | 93,328.9 | 36 | 36 | 479 | 100 | −2.44 | 0.010 | −3.32 | 0.010 | −5.38 | 0.005 |
| 29 | 76779293 | Keratin 8 | 5.70 | 54,513.5 | 29 | 59 | 723 | 100 | −4.51 | 0.013 | +2.18 | 0.027 | +1.66 | 0.077 |
| 39 | 198278553 | Myosin, light polypeptide 9, regulatory | 4.80 | 19,898.5 | 8 | 41 | 416 | 100 | −2.05 | 0.030 | +2.49 | 0.018 | +2.30 | 0.023 |
| 40 | 119850791 | Krt 78 protein | 5.97 | 55,423.6 | 3 | 6 | 100 | 99.999 | +3.24 | 0.003 | −1.80 | 0.050 | −2.10 | 0.029 |
| 44 | 49864 | Actin, aortic smooth muscle | 5.45 | 38,016 | 12 | 39 | 583 | 100 | −3.02 | 0.007 | −3.47 | 0.003 | −1.80 | 0.054 |
| *Oxidative stress* | | | | | | | | | | | | | | |
| 1 | 12805209 | Lectin, galactose binding, soluble 1 | 5.32 | 15,210.4 | 4 | 36 | 148 | 100 | +1.39 | 0.020 | −2.59 | 0.017 | −2.32 | 0.022 |
| 2 | 12805209 | Lectin, galactose binding, soluble 1 | 5.32 | 15,210.4 | 8 | 49 | 421 | 100 | +1.39 | 0.015 | +1.03 | 0.910 | −2.74 | 0.015 |
| 16 | 148747558 | Peroxiredoxin 2 | 5.20 | 21,936.1 | 6 | 28 | 181 | 100 | −3.04 | 0.008 | −1.07 | 0.755 | +1.23 | 0.043 |
| 19 | 6680117 | Glutathione synthetase | 5.56 | 52,442.0 | 27 | 53 | 773 | 100 | −2.79 | 0.007 | +1.27 | 0.317 | +1.58 | 0.098 |
| 23 | 148680717 | Thioredoxin-like 5, isoform CRA_a | 4.56 | 8661.1 | 1 | 18 | 75 | 99.507 | +1.03 | 0.096 | −3.51 | 0.009 | −3.38 | 0.009 |
| 34 | 165932331 | Lactoylglutathione lyase | 5.24 | 20,967.4 | 13 | 56 | 693 | 100 | +1.12 | 0.602 | −1.63 | 0.084 | −5.38 | 0.005 |
| 47 | 45597447 | Cu/Zn Superoxide dismutase | 6.03 | 15,922.8 | 7 | 43 | 403 | 100 | +1.22 | 0.154 | −5.29 | 0.005 | −4.41 | 0.006 |
| *Signal transduction* | | | | | | | | | | | | | | |
| 3 | 27501448 | Eukaryotic translation initiation factor 6 | 4.63 | 27,007.4 | 5 | 27 | 276 | 100 | +3.00 | 0.003 | −1.53 | 0.112 | −1.21 | 0.396 |
| 4 | 5803225 | 14-3-3 protein epsilon | 4.63 | 29,326.5 | 9 | 37 | 204 | 100 | −1.91 | 0.018 | −2.06 | 0.033 | +1.07 | 0.773 |
| 7 | 205371731 | Serine protease inhibitor | 5.25 | 45,965.5 | 11 | 31 | 316 | 100 | +1.58 | 0.020 | −1.714 | 0.072 | −4.90 | 0.006 |
| 10 | 62024907 | Ribosomal protein SA | 4.80 | 32,935.5 | 17 | 61 | 1020 | 100 | −5.83 | 0.006 | +1.24 | 0.852 | +1.35 | 0.222 |
| 18 | 4503529 | Eukaryotic initiation factor 4A-1 | 5.32 | 46,352.6 | 23 | 54 | 677 | 100 | −3.47 | 0.005 | −1.67 | 0.077 | +1.26 | 0.321 |
| 21 | 58476100 | Heterogeneous nuclear ribonucleoprotein F | 5.30 | 43,943.0 | 8 | 20 | 247 | 100 | +3.13 | 0.004 | −1.21 | 0.407 | +1.12 | 0.606 |
| 22 | 58476100 | Heterogeneous nuclear ribonucleoprotein F | 5.30 | 43,943.0 | 10 | 21 | 332 | 100 | +2.63 | 0.004 | −1.11 | 0.642 | +1.04 | 0.874 |
| 24 | 3065925 | 14-3-3 protein beta | 4.78 | 28,192.9 | 15 | 49 | 467 | 100 | −1.07 | 0.238 | −3.54 | 0.009 | −2.12 | 0.030 |
| 32 | 148682303 | Lysophospholipase 1, isoform CRA_c | 5.91 | 19,460.8 | 5 | 42 | 166 | 100 | −2.53 | 0.012 | −2.70 | 0.003 | +1.17 | 0.494 |
| 33 | 148702066 | mCG7879, isoform CRA_a | 4.75 | 29,294.6 | 12 | 37 | 422 | 100 | −2.02 | 0.010 | −2.88 | 0.013 | −2.43 | 0.020 |
| 43 | 6671569 | 60S acidic ribosomal protein P0 | 5.91 | 34,365.8 | 21 | 70 | 1480 | 100 | −4.69 | 0.005 | +1.48 | 0.912 | +1.18 | 0.470 |
| 46 | 148680528 | Eukaryotic translation initiation factor 5A, isoform CRA_a | 5.12 | 12,466.1 | 5 | 58 | 293 | 100 | −1.85 | 0.038 | +1.15 | 0.536 | +1.59 | 0.096 |
| 52 | 12805513 | Eef2 protein | 6.36 | 32,378.4 | 18 | 73 | 765 | 100 | −1.19 | 0.584 | −5.76 | 0.005 | −1.79 | 0.055 |
| 58 | 3065929 | 14-3-3 protein gamma | 4.80 | 28,516.0 | 14 | 43 | 443 | 100 | −1.51 | 0.047 | −2.79 | 0.014 | −1.97 | 0.038 |

[a] Spot ID represents the protein spot number on the 2-D DIGE gels.
[b] Accession numbers according to the NCBI database.
[c] Spot abundance is expressed as the average ratio of intensities of up-regulated (positive values) or down-regulated (negative values) proteins at 0, 3, 6 and 24 h after OA treatment.

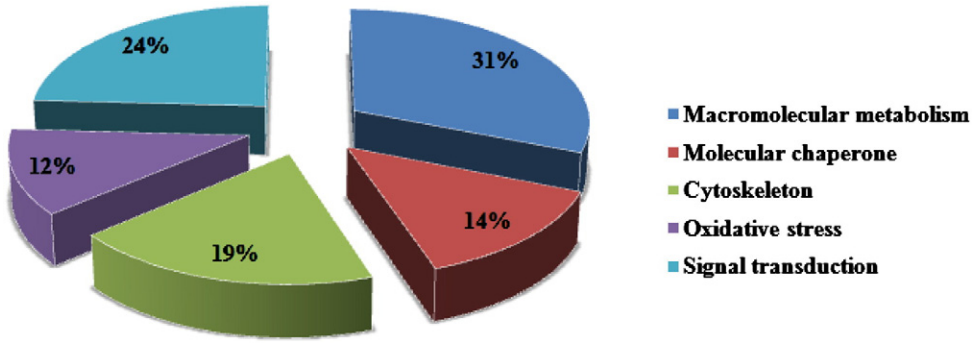


**Fig. 5 – Functional distribution of altered proteins in intestinal tissues of ICR mice at 0 h, 3 h, 6 h and 24 h after a single oral administration of OA (750 μg/kg body weight).**

urea cycle, ornithine participates in several reactions that help ensure the proper balance of protein building blocks (amino acids) in the body. Spermidine synthase (spot 50) and adenosine kinase (spot 54) were down-regulated 6 h and 24h after oral administration. The former is one of the four enzymes in the polyamine-biosynthetic pathway and carries out the final step of spermidine biosynthesis, the latter plays a key role in catalyzing the phosphorylation of ribofurnosyl-containing nucleoside analogues at the 5′-hydroxyl position using ATP or GTP as the phosphate donor and maintains the energy homeostasis. The present results suggested that the down-regulation of these proteins at 6 h and/or 24 h might be due to the negative nitrogen balance induced by the diarrhea caused by the OA treatment.

Epithelial cells display distinct structural and functional attributes and serve both as a physiological and structural barrier. The microvilli are believed to increase cell surface area thus regulating the absorptive and secretory functions of epithelial cells. Recently, OA was proved to cause rapid changes in the structural organization of the intermediate filament, followed by a loss of microtubules, solubilization of intermediate filament proteins, and disruption of desmosomes [39–41]. So it is not surprising that a total of 11 cytoskeleton reorganization related proteins were altered after oral administration of OA and most of them were down-regulated. These proteins included keratins, villin 1, myosin regulatory light polypeptide 9 and actin. Among these altered proteins, villin 1 (spot 26 and 27) was down-regulated during the entire experimental period. Villin is an epithelial cell-specific protein and belongs to a family of actin-binding proteins, which is associated with actin filaments in the microvilli and terminal web of epithelial cells. One study demonstrates that villin plays important roles in regulating actin dynamics, cell morphology, cell mobility, cell migration and cell survival [42]. Moreover, villin is also involved in the initial organization and formation of the microvilli [43]. As part of the epithelial cytoskeleton, keratins are important for the mechanical stability and integrity of epithelial cells and tissues. Some keratins also have regulatory functions and are involved in intracellular signaling pathways, *e.g.* protection from stress, wound healing, and apoptosis [44]. In our study, several keratins (keratin 7, 8 and 19) were identified and most of them were down-regulated during the entire experimental period, especially EndoA' cytokeratin (spot 12), suggesting that OA

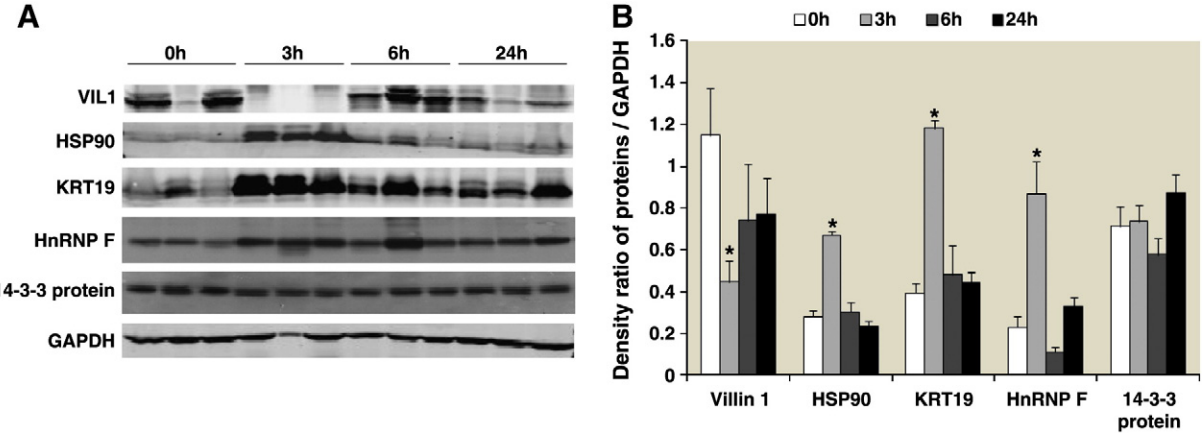


**Fig. 6 – Western blot analysis of five selected proteins in the intestinal tissues of ICR mice at 0 h, 3 h, 6 h and 24 h after a single oral administration of OA (750 μg/kg body weight). Intensities of the proteins were normalized to the corresponding GAPDH level. Values are given as means ± SD ($n$ = 3).A: Representative western blots, B: Western blot results from densitometry analysis. *$p < 0.05$.**

could induce the functional secretory disturbance of the intestinal gland. The present study demonstrated that the down-regulation by OA of cytoskeletal proteins, especially villin 1 and EndoA' cytokeratin, affected actin dynamics and the microfilament network, and subsequently interrupted cytoskeleton reorganization of intestinal epithelial cells. Evidence from morphological changes of microvilli (Fig. 3A) in the present study also confirmed the toxic effects of OA on epithelial cells.

Homeostatic balance between proliferation and apoptosis is essential for the intestinal epithelium to function as a physiological and structural barrier. Intestinal epithelial cells have a high turnover rate as well as a high apoptosis rate. A recent study indicates that the physiological function of villin is not only as a cytoskeletal protein, but also as an epithelial cell-specific anti-apoptotic protein and it can protect cells from apoptosis by maintaining mitochondrial integrity and thus inhibiting the activation of caspase-9 and caspase-3 [45]. Many studies demonstrate that apoptosis is induced by OA through the inhibition of PP1 and PP2A activities [46–50]. Our study found that the down-regulation of villin was accompanied by damage of mitochondrial structure, suggesting that villin might play a key role in inducing the apoptosis of epithelial cells by OA. In addition, calcium ions are recognized as an important regulator in the signal transduction pathway of apoptosis, and calcium homeostasis is an important mechanism involved in neurodegenerative and aging processes [51,52]. As a $Ca^{2+}$ binding protein, villin might induce apoptosis *via* the $Ca^{2+}$-induced cell death pathway in OA-treated intestines. Thus, villin might play a key role in the OA induced diarrhea of mice and could be used as a candidate biomarker for acute OA toxicity.

Apart from villin, other apoptosis-related proteins were also found to alter significantly in OA-treated intestines, *i.e.* 14-3-3 proteins and eIFs. The 14-3-3 proteins are a group of dimeric acidic proteins with a relative molecular mass of 30 kDa and are relatively conserved in all eukaryotes. Studies demonstrate that the 14-3-3 epsilon protein is one of the caspase-3 substrates, and the cleavage of 14-3-3 protein can promote cell death by releasing the associated BAD from the 14-3-3 protein, and so facilitate BAD translocation to the mitochondria and its interaction with Bcl-x [53]. In our study, three isoforms of 14-3-3 protein were identified and the expressions of two isoforms (spot 4 and spot 58) were down-regulated at 3 h after OA exposure. We speculated that the down-regulation of 14-3-3 proteins might have led to cytoplasmic release of phosphorylated BAD protein and so induced apoptosis. Recent studies indicate that PP1 and PP2A are important regulators of 14-3-3 binding interactions, and PP2A contributes to the regulation of 14-3-3 binding to the pro-apoptotic agent BAD and to two components of the Ras signal transduction [54–56]. The eIFs are proteins which regulate protein synthesis in cells. Some of them play an important role in the association

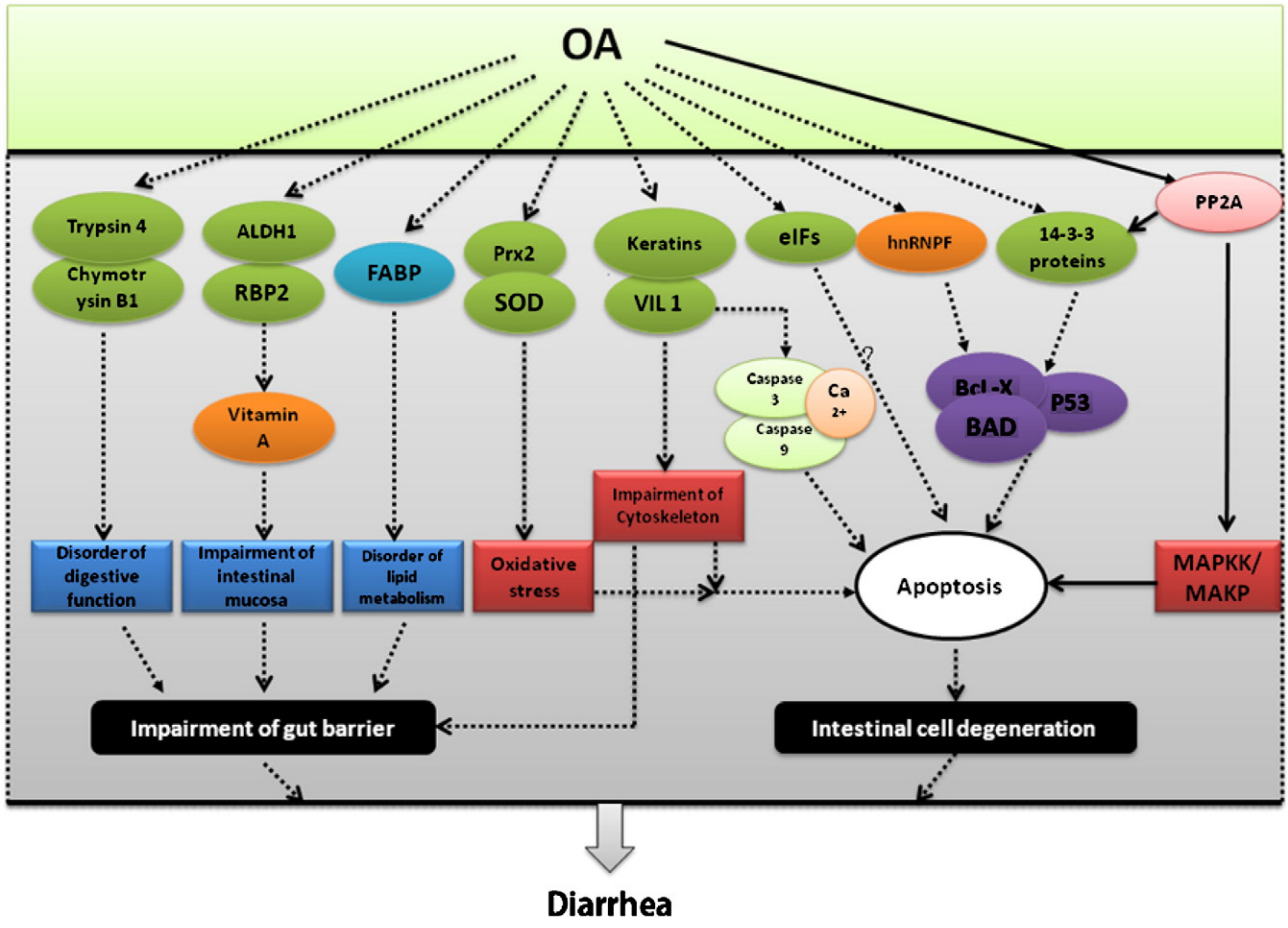


**Fig. 7 – The proposed scheme illustrating cellular events in intestinal tissues of ICR mice after a single oral administration of OA.**

or dissociation of the ribosomal subunit for the translation of the mRNA into protein, and are involved in cell stress response. Many studies report that the eIFs play an important role in cell apoptosis [57,58]. Among of them, eIF6 is believed to be part of a mechanism acting on the specific translation of messengers regulating cell survival [59]. An over-expression of eIF5A1 results in the loss of mitochondrial transmembrane potential, translocation of Bax to the mitochondria, release of cytochrome c, caspase activation, up-regulation of p53, and up-regulation of Bim [57]. Thus, the down-regulation of eIFs in our study indicated that OA might have induced the apoptosis of epithelial cells. Nevertheless, the results in this study suggested that OA caused intestinal dysfunction in mice *via* destroying the cytoskeleton and inducing apoptosis of intestinal epithelial cells, thus resulting in diarrhea.

One interesting finding of this study was that a new protein, hnRNP F, was induced by OA 3 h after oral administration but it was not found at other time points. hnRNP F is an RNA binding protein which is associated with pre-mRNAs in the nucleus and regulates alternative splicing, polyadenylation, and other aspects of mRNA metabolism and transport [60]. Previous studies demonstrate that hnRNP F might be involved in apoptotic signal pathways, and play a positive role in the production of the proapoptotic regulator Bcl-x (S.) [61]. The induction of hnRNP F 3 h after oral administration indicated that hnRNP F might promote the apoptotic progress of intestinal cells under OA stress, degenerate the gut barrier function, and then induce diarrhea.

Recent studies indicate that OA induces oxidative stress in mice brains, characterized by a high level of lipid peroxidation and decreases in GSH content and that it destroys the activities of antioxidative enzymes [62]. Moreover, OA induces apoptosis *via* increasing reactive oxygen species (ROS), protein carbonylation, lipid peroxidation, caspase-3 activity, and mitochondrial dysfunction in many cell types [46,47]. Our proteomic analysis found that seven proteins related with oxidative stress altered significantly in OA-treated mice. Two antioxidative enzymes, antioxidant protein PRX2 and Cu/Zn SOD, were down-regulated 3 h and 6 h after OA oral administration, respectively. PRX2 is a ubiquitously expressed thiol-specific antioxidant enzyme that catalyzes the degradation of $H_2O_2$ and other ROS, while Cu/Zn SOD is an important enzyme involved in antioxidant defense in nearly all cells through catalyzing the dismutation of superoxide into oxygen and hydrogen peroxide. As the third most abundant protein in erythrocytes, PRX2 competes effectively with catalase and glutathione peroxidase to scavenge low levels of hydrogen peroxide, including that derived from hemoglobin autoxidation. It is possible that oxidation represents an alternative mechanism for stimulating cellular responses relevant to the diarrhetic effects of OA. In addition, our results found that eight molecular chaperone proteins were altered in expression by OA. Heat shock proteins (HSPs) are highly regulated proteins that are involved in normal cellular activity, and are up-regulated when the cell is exposed to stress such as heat or excess ROS production [63]. Our results showed that the protein level of HSPs increased at 3 h, but decreased at 6 h and 24 h. These results suggested that OA might induce excess ROS production in the intestine especially 3 h after oral administration, which depressed the expression of antioxidative enzymes and enhanced the expression of HSPs, and subsequently destroyed the antioxidant defense barrier of the mouse intestines.

## 5. Conclusions

The present study provided a new insight at the proteomic level into the acute toxicity of OA on mouse intestines. The presence of OA destroyed the intestinal microvilli and cellular ultrastructure (rER and mitochondria), and also inhibited PP activity significantly, which resulted in the dephosphorylation of numerous proteins regulating essential metabolic processes in intestinal cells, and subsequently to diarrhea. The proteomic analysis revealed that OA toxicity destroyed the digestive enzyme system, affecting lipid, amino acid and sugar metabolism, cytoskeleton reorganization, and inducing oxidative stress with a concomitant interference with cell signal transduction in the intestinal cells, suggesting that OA toxicity in mouse intestines is complex and diverse, and multiple proteins and biological processes are involved in the diarrhetic process (Fig. 7). Villin 1 and hnRNP F might be the key triggers inducing diarrhea *via* interrupting cytoskeleton reorganization and cell apoptosis in the mouse small intestines, and could be used as candidate biomarkers for acute OA toxicity. However, it is worth noting that the adverse effects of OA were short and the small intestine could recover its normal functions gradually within 24 h.

## Acknowledgments

This work was supported by the State Key Laboratory of Marine Environmental Science (Xiamen University), the National Natural Science Foundation of China (No. 41106092), and the Program for New Century Excellent Talents in Universities of China to D.-Z. Wang. The authors thank Prof. John Hodgkiss, the University of Hong Kong for helping to revise the manuscript.

## Appendix A. Supplementary data

Supplementary data to this article can be found online at doi:10.1016/j.jprot.2012.01.010.

## REFERENCES

[1] Yasumoto T, Oshima Y, Yamaguchi M. Occurrence of a new type of shellfish poisoning in the Tohoku District. Bull Jpn Soc Sci Fish 1978;44:1249–55.
[2] Chen HC. Seafood microorganisms and seafood safety. J Food Drug Anal 1995;3:133–44.
[3] Van Dolah FM. Marine algal toxins: origins, health effects, and their increased occurrence. Environ Health Perspect 2000;108:133–41.
[4] Ito E, Satake M, Ofuji K, Kurita N, McMahon T, James K, et al. Multiple organ damage caused by a new toxin azaspiracid, isolated from mussels produced in Ireland. Toxicon 2000;38:917–30.
[5] Ito E, Terao K. Injury and recovery process of intestine caused by okadaic acid and related compounds. Nat Toxins 1994;2:371–7.
[6] Cohen P, Holmes CF, Tsukitani Y. Okadaic acid: a new probe for the study of cellular regulation. Trends Biochem Sci 1990;15:98–102.

[7] Bialojan C, Takai A. Inhibitory effect of a marine-sponge toxin, okadaic acid, on protein phosphatases. Specificity and kinetics. Biochem J 1988;256:283–90.
[8] Aonuma S, Ushijima T, Nakayasu M, Shima H, Sugimura T, Nagao M. Mutation induction by okadaic acid, a protein phosphatase inhibitor, in CHL cells, but not in *S. typhimurium*. Mutat Res 1991;250:375–81.
[9] Fujiki H, Suganuma M. Tumor promotion by inhibitors of protein phosphatases 1 and 2A: the okadaic acid class of compounds. Adv Cancer Res 1993;61:143–94.
[10] Fujiki H, Suganuma M, Nishiwaki S, Yoshizawa S, Yatsunami J, Matsushima R, et al. Specific mechanistic aspects of animal tumor promoters: the okadaic acid pathway. Prog Clin Biol Res 1992;374:337–50.
[11] Fujiki H, Suganuma M, Yoshizawa S, Nishiwaki S, Winyar B, Sugimura T. Mechanisms of action of okadaic acid class tumor promoters on mouse skin. Environ Health Perspect 1991;93:211–4.
[12] Goto KFJ, Haneji T. Okadaic acid stimulates apoptosis through expression of Fas receptor and Fas ligand in human oral squamous carcinoma cells. Oral Oncol 2002;38:16–22.
[13] Parameswaran N, Spielman WS, Brooks DP, Nambi P. Okadaic acid stimulates caspase-like activities and induces apoptosis of cultured rat mesangial cells. Mol Cell Biochem 2004;260: 7–11.
[14] Li Z, Tu X, Wang CC. Okadaic acid overcomes the blocked cell cycle caused by depleting Cdc2-related kinases in *Trypanosoma brucei*. Exp Cell Res 2006;312:3504–16.
[15] Ray RM, Bhattacharya S, Johnson LR. Protein phosphatase 2A regulates apoptosis in intestinal epithelial cells. J Biol Chem 2005;280:31091–100.
[16] Gehringer MM. Microcystin-LR and okadaic acid-induced cellular effects: a dualistic response. FEBS Lett 2004;557:1–8.
[17] Ao L, Liu JY, Gao LH, Liu SX, Yang MS, Huang MH, et al. Differential expression of genes associated with cell proliferation and apoptosis induced by okadaic acid during the transformation process of BALB/c 3T3 cells. Toxicol In Vitro 2008;22:116–27.
[18] Escoffier N, Gaudin J, Mezhoud K, Huet H, Chateau-Joubert S, Turquet J, et al. Toxicity to medaka fish embryo development of okadaic acid and crude extracts of *Prorocentrum* dinoflagellates. Toxicon 2007;49:1182–92.
[19] Tubaro A, Sosa S, Altinie G, Soranzo MR, Satake M, Della Loggia R, et al. Short-term oral toxicity of homoyessotoxins, yessotoxin and okadaic acid in mice. Toxicon 2004;43:439–45.
[20] Hoorn EJ, Hoffert JD, Knepper MA. The application of DIGE-based proteomics to renal physiology. Nephron Physiol 2006;104:61–72.
[21] Dowling VA, Sheehan D. Proteomics as a route to identification of toxicity targets in environmental toxicology. Proteomics 2006;6:5597–604.
[22] Tubaro A, Sosa S, Carbonatto M, Altinier G, Vita F, Melato M, et al. Oral and intraperitoneal acute toxicity studies of yessotoxin and homoyessotoxins in mice. Toxicon 2003;41: 783–92.
[23] Fernandez Puente P, Fidalgo Saez MJ, Hamilton B, Lehane M, Ramstad H, Furey A, et al. Rapid determination of polyether marine toxins using liquid chromatography–multiple tandem mass spectrometry. J Chromatogr A 2004;1056:77–82.
[24] Toshiyuki S, Akira M, Katsuhisa B, Rieko S, Takashi K. LC–MS/MS analysis of okadaic acid analogues and other lipophilic toxins in single-cell isolates of several *Dinophysis* species collected in Hokkaido, Japan. Harmful Algae 2009;8: 233–8.
[25] Fontal OI, Vieytes MR, Baptista de Sousa JM, Louzao MC, Botana LM. A fluorescent microplate assay for microcystin-LR. Anal Biochem 1999;269:289–96.
[26] Vieytes MR, Fontal OI, Leira F, Baptista de Sousa JM, Baptista de Sousa LM. A fluorescent microplate assay for diarrheic shellfish toxins. Anal Biochem 1997;248:258–64.
[27] Friedman DB, Hill S, Keller JW, Merchant NB, Levy SE, Coffey RJ, et al. Proteome analysis of human colon cancer by two-dimensional difference gel electrophoresis and mass spectrometry. Proteomics 2004;4:793–811.
[28] Wang MH, Chan LL, Si MZ, Hong HS, Wang DZ. Proteomic analysis of hepatic tissue of zebrafish (*Danio rerio*) experimentally exposed to chronic microcystin-LR. Toxicol Sci 2010;113:60–9.
[29] Wang MH, Wang DZ, Lin L, Hong HS. Protein profiles in zebrafish (Danio rerio) brains exposed to chronic microcystin-LR. Chemosphere 2010;81:716–24.
[30] Ito E, Yasumoto T, Takai A, Imanishi S, Harada K. Investigation of the distribution and excretion of okadaic acid in mice using immunostaining method. Toxicon 2002;40: 159–65.
[31] Terao K, Ito E, Yanagi T, Yasumoto T. Histopathological studies on experimental marine toxin poisoning. I. Ultrastructural changes in the small intestine and liver of suckling mice induced by dinophysistoxin-1 and pectenotoxin-1. Toxicon 1986;24:1141–51.
[32] Stoker AW. Protein tyrosine phosphatases and signalling. J Endocrinol 2005;185:19–33.
[33] Storch J, McDermott L. Structural and functional analysis of fatty acid-binding proteins. J Lipid Res 2009;50:S126–31.
[34] Levy E, Mehran M, Seidman E. Caco-2 cells as a model for intestinal lipoprotein synthesis and secretion. FASEB J 1995;9: 626–35.
[35] Kanai M, Raz A, Goodman DS. Retinol-binding protein: the transport protein for vitamin A in human plasma. J Clin Invest 1968;47:2025–44.
[36] Jin L, Xiao CL, Lu CH, Xia M, Xing GW, Xiong S, et al. Transcriptomic and proteomic approach to studying SNX-2112-induced K562 cells apoptosis and anti-leukemia activity in K562-NOD/SCID mice. FEBS Lett 2009;583:1859–66.
[37] Marquardt T, Freeze H. Congenital disorders of glycosylation: glycosylation defects in man and biological models for their study. Biol Chem 2001;382:161–77.
[38] Ventura G, De Bandt JP, Segaud F, Perret C, Robic D, Levillain O, et al. Overexpression of ornithine aminotransferase: consequences on amino acid homeostasis. Br J Nutr 2009;101: 843–51.
[39] Vilarino N, Ares IR, Cagide E, Louzao MC, Vieytes MR, Yasumoto T, et al. Induction of actin cytoskeleton rearrangement by methyl okadaate—comparison with okadaic acid. FEBS J 2008;275:926–34.
[40] Vale C, Botana LM. Marine toxins and the cytoskeleton: okadaic acid and *Dinophysis* toxins. FEBS J 2008;275:6060–6.
[41] Espina B, Rubiolo JA. Marine toxins and the cytoskeleton: pectenotoxins, unusual macrolides that disrupt actin. FEBS J 2008;275:6082–8.
[42] Khurana S, George SP. Regulation of cell structure and function by actin-binding proteins: villin's perspective. FEBS Lett 2008;582:2128–39.
[43] Heintzelman MB, Mooseker MS. Assembly of the intestinal brush border cytoskeleton. Curr Top Dev Biol 1992;26:93–122.
[44] Moll R, Divo M, Langbein L. The human keratins: biology and pathology. Histochem Cell Biol 2008;129:705–33.
[45] Wang Y, Srinivasan K, Siddiqui MR, George SP, Tomar A, Khurana S. A novel role for villin in intestinal epithelial cell survival and homeostasis. J Biol Chem 2008;283:9454–64.
[46] Xing ML, Wang XF, Zhu X, Zhou XD, Xu LH. Morphological and biochemical changes associated with apoptosis induced by okadaic acid in human amniotic FL cells. Environ Toxicol 2009;24:437–45.

[47] Jayaraj R, Gupta N, Rao PV. Multiple signal transduction pathways in okadaic acid induced apoptosis in HeLa cells. Toxicology 2009;256:118–27.
[48] Rami BG, Chin LS, Lazio BE, Singh SK. Okadaic-acid-induced apoptosis in malignant glioma cells. Neurosurg Focus 2003;14:e4.
[49] Elegbede JA, Hayes K, Schell K, Oberley TD, Verma AK. Induction of apoptosis and inhibition of papilloma formation may signal a new role for okadaic acid. Life Sci 2002;71: 421–36.
[50] Li DW, Fass U, Huizar I, Spector A. Okadaic acid-induced lens epithelial cell apoptosis requires inhibition of phosphatase-1 and is associated with induction of gene expression including p53 and bax. Eur J Biochem 1998;257:351–61.
[51] Timmins JM, Ozcan L, Seimon TA, Li G, Malagelada C, Backs J, et al. Calcium/calmodulin-dependent protein kinase II links ER stress with Fas and mitochondrial apoptosis pathways. J Clin Invest 2009;119:2925–41.
[52] Smaili S, Hirata H, Ureshino R, Monteforte PT, Morales AP, Muler ML, et al. Calcium and cell death signaling in neurodegeneration and aging. An Acad Bras Cienc 2009;81: 467–75.
[53] Won J, Kim DY, La M, Kim D, Meadows GG, Joe CO. Cleavage of 14-3-3 protein by caspase-3 facilitates bad interaction with Bcl-x(L) during apoptosis. J Biol Chem 2003;278:19347–51.
[54] Chiang CW, Kanies C, Kim KW, Fang WB, Parkhurst C, Xie M, et al. Protein phosphatase 2A dephosphorylation of phosphoserine 112 plays the gatekeeper role for BAD-mediated apoptosis. Mol Cell Biol 2003;23:6350–62.
[55] Ory S, Zhou M, Conrads TP, Veenstra TD, Morrison DK. Protein phosphatase 2A positively regulates Ras signaling by dephosphorylating KSR1 and Raf-1 on critical 14-3-3 binding sites. Curr Biol 2003;13:1356–64.
[56] Dougherty MK, Morrison DK. Unlocking the code of 14-3-3. J Cell Sci 2004;117:1875–84.
[57] Sun Z, Cheng Z, Taylor CA, McConkey BJ, Thompson JE. Apoptosis induction by eIF5A1 involves activation of the intrinsic mitochondrial pathway. J Cell Physiol 2010;223: 798–809.
[58] Shahbazian D, Parsyan A, Petroulakis E, Topisirovic I, Martineau Y, Gibbs BF, et al. Control of cell survival and proliferation by mammalian eukaryotic initiation factor 4B. Mol Cell Biol 2010;30:1478–85.
[59] De Marco N, Iannone L, Carotenuto R, Biffo S, Vitale A, Campanella C. p27(BBP)/eIF6 acts as an anti-apoptotic factor upstream of Bcl-2 during *Xenopus laevis* development. Cell Death Differ 2009;17:360–72.
[60] Wei CC, Guo DF, Zhang SL, Ingelfinger JR, Chan JS. Heterogenous nuclear ribonucleoprotein F modulates angiotensinogen gene expression in rat kidney proximal tubular cells. J Am Soc Nephrol 2005;16:616–28.
[61] Garneau D, Revil T, Fisette JF, Chabot B. Heterogeneous nuclear ribonucleoprotein F/H proteins modulate the alternative splicing of the apoptotic mediator Bcl-x. J Biol Chem 2005;280:22641–50.
[62] Tunez I, Munoz Mdel C, Feijoo M, Munoz-Castaneda JR, Bujalance I, Valdelvira ME, et al. Protective melatonin effect on oxidative stress induced by okadaic acid into rat brain. J Pineal Res 2003;34:265–8.
[63] Di Domenico F, Sultana R, Tiu GF, Scheff NN, Perluigi M, Cini C, et al. Protein levels of heat shock proteins 27, 32, 60, 70, 90 and thioredoxin-1 in amnestic mild cognitive impairment: an investigation on the role of cellular stress response in the progression of Alzheimer disease. Brain Res 2010;1333:72–81.